doi:10.1038/nature11771

1. The Ni Content of Mantle Peridotite and Its Primary Magmas

Of the 590 whole rock spinel and garnet peridotite analyses from off-craton xenolith and tectonic occurrences compiled by Herzberg (1993), 407 contain Ni data and these are shown in Fig. S1. Fertile peridotite has 0.03% K_2O (McDonough and Sun, 1995), and most of the peridotites have higher K_2O, indicating that they were modified by metasomatism. There are 264 analyses with K_2O < 0.03%, and these generally have more uniform NiO contents than the metasomatised types. Nevertheless, many of the measurements in this database were obtained in the 1960s by analytical methods that predated the XRFS, and the variation in Ni shown in Fig. S1 likely reflects uncertainties in analytical method. For example, peridotites with K_2O < 0.03% can be described by the equation: Ni (ppm) = 71.7MgO – 844, and the uncertainty is ± 254 ppm (1σ).

The old database of Herzberg (1993) can now be compared with the more recent determinations of off-craton peridotite xenoliths from Asia (Ionov, 2007; 2010; Ionov and Hofmann, 2007; Ionov et al., 2005). Most Ionov data were obtained using wavelength-dispersive X-ray fluorescence spectrometry at the University of Mainz. Data quality is greatly improved (Fig. S1), and can be described by the equation: Ni (ppm) = 68.6MgO – 630 where the uncertainty of 110 fertile and depleted peridotite compositions is ± 46 ppm (1σ). Using this equation and 37.7% MgO in pyrolite (McDonough and Sun, 1995), we obtain 1957 ppm Ni, virtually indistinguishable from the McDonough and Sun (1995) canonical value of 1960 ppm.

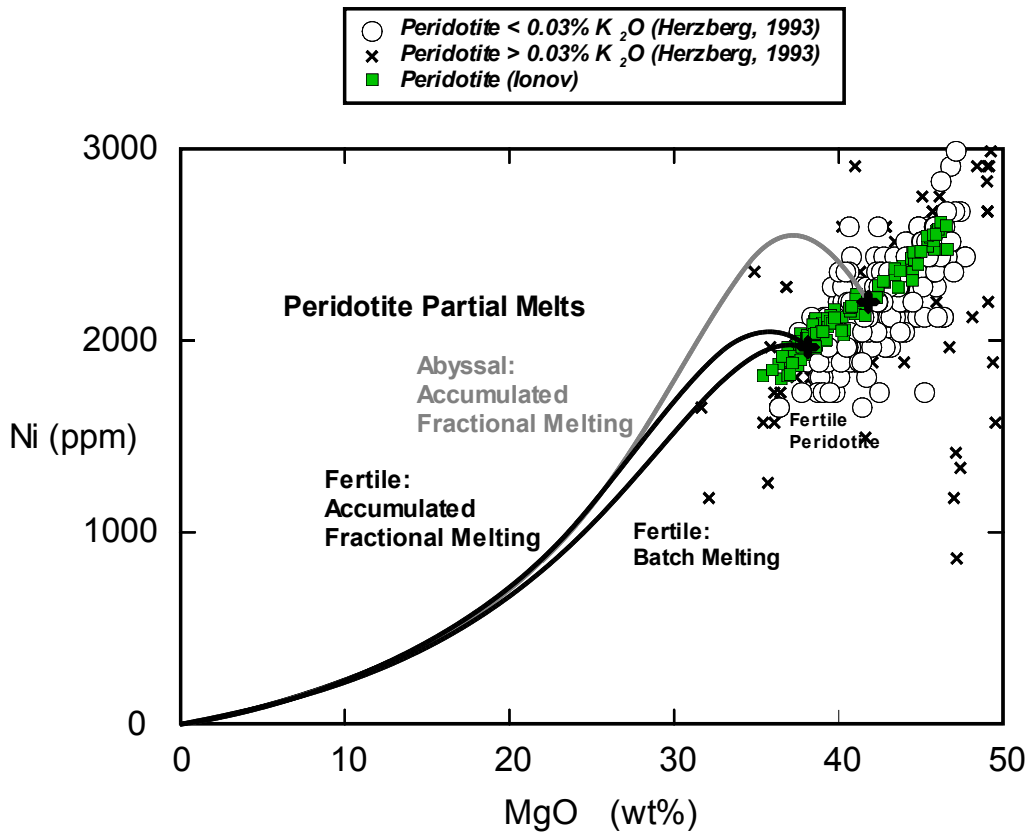

Figure S1. MgO and Ni contents of mantle peridotite and partial melts of mantle peridotite (Herzberg, 2011).

2. High Precision Olivine Analyses in Peridotite

Ionov (2007, 2010) and Ionov et al. (2005) published high-precision analyses of olivine in intraplate peridotite xenoliths from Tariat (Mongolia) and Tok (SE Siberia), and subduction xenoliths from Avacha (Kamchatka), using protocols similar to those reported by Sobolev et al. (2007). We have compiled these data and add high precision analyses of olivine from other off-craton spinel and garnet peridotites from Asia. Results from abyssal peridotites will be reported by Ionov and Sobolev separately, and are similar to intraplate and subduction occurrences, demonstrating homogeneity of Ni in all tectonic settings. Table S1 lists individual olivine analyses in some cases and also averages. Replicate analyses using the method of Sobolev et al. (2007) are in good agreement, and will be reported elsewhere by Ionov and Sobolev. Results of 203 analyses shown in Fig. 1 of the text reveal substantial homogeneity of Ni in peridotite olivine. They are in excellent agreement with model Ni contents of olivine (Fig. 1; Herzberg, 2011), although they are slightly higher in Ni in some cases, indicating the possible influence of Ni exchange with orthopyroxene on cooling (Herzberg, 1999). Overall olivine Ni homogeneity is in contrast with a wide range of Ni contents in olivines from peridotites compiled by Putirka et al. (2011) from GEOROC. While we concur that Ni-rich peridotite sources can be important in intraplate magmatism, we conclude the evidence for it can be weak in existing peridotite databases owing to questionable accuracy.

3. The Effects of Temperature, Pressure and Composition on the Partitioning of Ni between Olivine and Liquid

The partitioning of Ni between olivine and liquid depends on temperature, pressure, and composition of the melt (Hart and Davis, 1978; Beattie et al., 1991; Herzberg and Zhang, 1996; Wang and Gaetani, 2008; Filiberto et al., 2009; Putirka et al., 2011; Li and Ripley, 2010; Longhi et al., 2010; Niu et al., 2011). In particular, $D_{Ni}^{Ol/L}$ goes down with increasing MgO content of the melt. But as increasing temperatures and pressures of melting yield melts with higher MgO contents (O'Hara, 1968), it can be difficult to resolve the separate T-P-X effects. This problem has given rise to a plethora of parameterizations of experimental data that have calibrated $D_{Ni}^{Ol/L}$ as a function of T-P-X. It is important to resolve because elevated Ni contents of olivine phenocrysts have been used to infer pyroxenite melting in the source (Sobolev et al., 2005; 2007; Herzberg, 2011), elevated temperatures and pressures in mantle plumes (Li and Ripley, 2010; Putirka et al., 2011; Matzen et al., 2012) and elevated pressures (Niu et al., 2011).

We adopt a model of Ni partitioning that provides the minimum error when recovering experimental data. This is a temperature-independent model first formulated by Jones (1984), later calibrated by Beattie et al. (1991), and corroborated in subsequent studies (Wang and Gaetani, 2008; Filberto et al., 2009; Longhi et al., 2010). We call this a Beattie-Jones model, which is described by:

$$D_{NiO}^{Ol/L} = NiO^{OL}/NiO^{L} \quad (1)$$

$$D_{MgO}^{OL} = MgO^{Ol}/MgO^{L} \quad (2)$$

and

$$D_{NiO}^{Ol/L} = 3.346\, D_{MgO}^{Ol/L} - 3.665 \quad (3)$$

where NiO^{OL}, NiO^{L}, MgO^{Ol}, MgO^{L} refer to mole fractions of NiO and MgO in the phases liquid (L) and olivine (Ol), based on one metal cation per oxide (i.e., SiO_2, MgO, $AlO_{1.5}$, $NaO_{0.5}$ etc.; Beattie ert al., 1991). The constants in equation (3) have been obtained from a parameterization of experimental data (Beattie et al., 1991), which we have tested using the experimental database on Fe-bearing compositions collated by Li and Ripley (2010). To this database was added:

- 11 experiments of Longhi et al. (2010; 1554 to 2015ºC and 1.6 to 6.0 GPa).
- 11 experiments of Taura et al. (1998; 1600 to 2000ºC and 3.0 to 14.4 GPa using both electron microprobe and SIMS analyses)
- 6 experiments of Le Roux et al. (2011; 1300 to 1500 ºC and 1.5 to 2.0 GPa)
- 10 experimens of Matzen et al. (2011; 1301 to 1500 ºC and 1 atmosphere)

There are a total of 271 experiments with temperatures in the 1122-2050ºC range and pressures in the 1 atmosphere to 13 GPa range. To these experiments, the olivine/liquid distribution coefficients $D_{NiO}^{Ol/L}$ were calculated according to the Beattie-Jones equation (3). For the entire database (N = 271) we calculate:

$$1 \text{ standard deviation } (1\sigma) = (\Sigma(D_{NiO},\text{calculated} - D\ D_{NiO},\text{observed})^2/(N-1))^{0.5} \quad (4)$$

and obtain 1σ = 1.1. However, the difference between calculated and observed $D_{NiO}^{Ol/L}$ is clearly related to temperature as shown in Fig. S2. This likely reflects the effects of temperature on promoting equilibrium during the course of an experiment, and differences between calculated and observed partitioning are minimized and approximately constant at T > 1500°C. We have developed an empirical expression for computing the effects of temperature on σ by binning the experimental database in 100°C increments. At T > 1500°C:

$$1 \text{ standard deviation } (1\sigma) = 0.4 \quad (5)$$

and T < 1500°C:

$$1 \text{ standard deviation } (1\sigma) = -9.308 + 0.0179T - 0.0000075T^2 \quad (6)$$

The results of this uncertainty analysis on the Ni content of olivine in equilibrium with partial melts of mantle peridotite was shown in Fig. 1 of the main body of this paper.

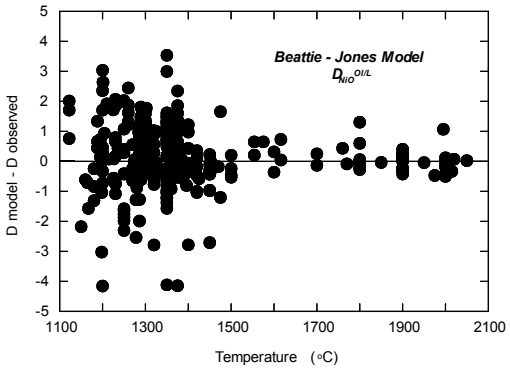

Figure S2. A comparison of model and experimentally observed partition coefficients for nickel.

It was shown by Herzberg (2011) that the method of Beattie et al. (1991; equation 3) provides a better description of experimental data than the method of Li and Ripley (2010) which contains independently adjustable temperature and composition terms. Similarly, Putirka et al. (2011) have expressed the partitioning of NiO on a weight % basis, and parameterized it according to both temperature (°C) and composition (wt%). They parameterized 81 experiments with:

$$D_{NiO}^{Ol/L} = \exp[-3.257 + 6800/T] \quad (7a)$$

49 experiments with:

$$D_{NiO}^{Ol/L} = \exp[-4.75 + 0.033(SiO_2)^L + 6829/T] \quad (7b)$$

and 81 experiments with:

$$D_{NiO}^{Ol/L} = \exp[-1.78 + .04(SiO_2)^L - 0.04(MgO)^L + 3236/T] \quad (7c)$$

These equations were labeled as 2a, 2b, and 2c in Putirka et al. (2011). Results shown in Fig. S3 demonstrate that the Beattie – Jones parameterization of equation (3) yields a more accurate description of the experimental database than Putirka et al. (2011). For mantle peridotite having 1960 ppm Ni that melts at high temperatures appropriate to a mantle plume, use of the Putirka et al. (2011) parameterization will yield primary magmas with Ni contents that are too high.

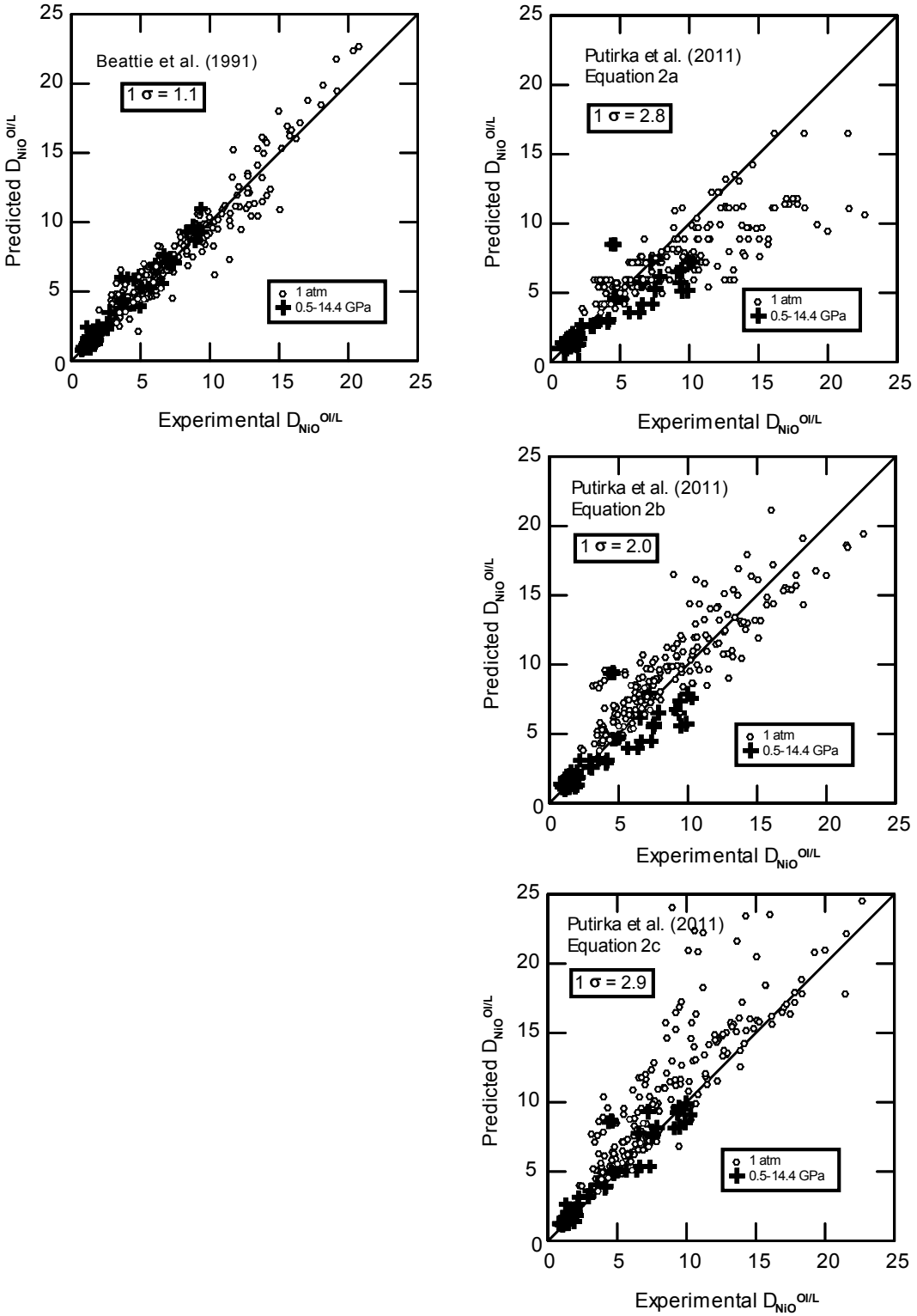

Figure S3. Measured versus calculated $D_{NiO}^{Ol/L}$ for equation (3) of Beattie et al. (1991) and equations 7a,b,c of Putirka et al. (2011).

Niu et al. (2011) suggested that the Ni content of olivine is a function of the pressure at which melting stops at the base of the lithosphere, which covers the 0 to 3 GPa range. They provided the following parameterization of a limited and unspecified number of experiments:

$$D_{NiO}^{Ol/L} = 4.6914P^{-0.5357} \quad (8)$$

As their equation (8) intercepts the y-axis at infinity, we restrict this analysis to experiments in the 0.5 to 3.2 GPa. Results shown in Fig. S4 demonstrate that the Niu et al. (2011) parameterization is not as successful as the method of Beattie et al. (1991) in describing the experimental database.

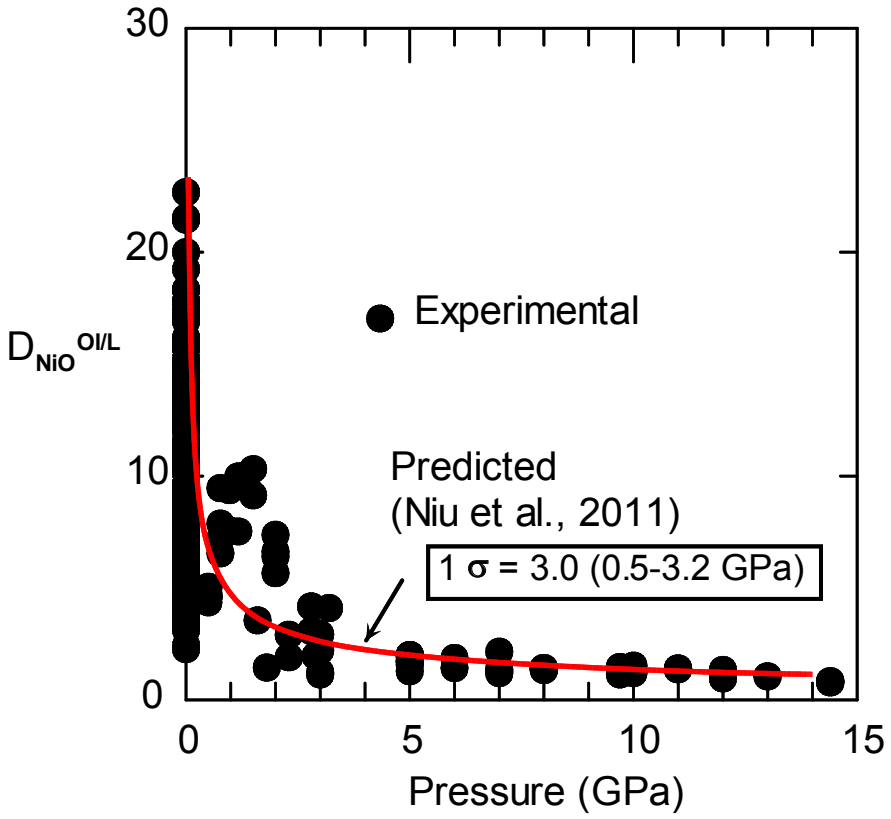

Figure S4. Measured versus calculated $D_{NiO}^{Ol/L}$ for equation (8) of Niu et al. (2011).

The most successful method for describing the Ni content of olivine phenocrysts to crystallize from magmas is provided by Beattie et al. (1991), and it is the one we have adopted in this work. The method has the advantage of requiring only the composition of the melt from which olivine crystallizes. There are no independently adjustable temperature and pressure terms, which are themselves model-dependent. We conclude that the high Ni contents of olivines in Baffin Island, Disko Island, West Greenland, the Ontong Java Plateau, Isla Gorgona, and Fernandina originated from a Ni-rich peridotite source, and are not artifacts of elevated temperatures and pressures of melting.

4. Forward Models of Liquid Lines of Descent Involving Olivine and Clinopyroxene

The problem of inferring source lithology is tractable when Mg-numbers of olivine phenocrysts are high, generally > 89 (Herzberg, 2011). For example, olivine phenocrysts for shield building lavas on Hawaii are higher in Ni and Fe/Mn, and lower in Mn and Ca than those expected of a normal peridotite source (Sobolev et al., 2005; 2007; Herzberg, 2011). In contrast, maximum Mg-numbers for olivine phenocrysts from many intraplate volcanoes are typically in the 80-88 range, and can result from the crystallization of both olivine and clinopyroxene from primary magmas. The problem is to compare high precision olivine analyses with those that are expected to crystallize from such magmas. This is solved by a forward model of the liquid line of descent, and the calculation of olivine that crystallizes along it.

The importance of sub Moho clinopyroxene fractionation in ocean island and MORB petrogenesis has been recognized previously (Albarède et al., 1997; Geist et al., 1998; Herzberg, 2004a; Herzberg and Asimow, 2008). The effect of decompression is to expand the liquidus crystallization fields of olivine and clinopyroxene (O'Hara, 1968; Herzberg, 1992), and both can crystallize when primary magmas interact with wall rocks during transit. Relative to olivine only crystallization, deep fractionation of clinopyroxene can produce derivative magmas with lower CaO, SiO_2, higher FeO, lower MnO, and higher NiO. Olivine that crystallizes from such melts at the surface will exhibit depletions in Ca and Mn, elevated Fe/Mn, and elevated Ni. The erroneous interpretation can be made that this olivine points to a pyroxenite source lithology even if the primary magmas melted from a peridotite source. The problem is how to distinguish the effects of clinopyroxene as a crystallizing phase from clinopyroxene a residual phase in pyroxenite source.

The method for calculating a liquid line of descent begins with identification of a primary magma composition. Primary magma compositions for peridotite-sources have been computed from primitive lava compositions that differed by olivine addition and subtraction using PRIMELT2 (Herzberg and Asimow, 2008). Results for many ocean islands and large igneous provinces were reported by Herzberg and Gazel (2009). In most cases it was sufficient to obtain primary magmas from the raw lava compositions. For Fernandina, most lava compositions were too differentiated to obtain primary magma compositions owing to plagioclase and augite fractionation. The few remaining primitive samples had unusually variable Mn, and primary magma Mn was adjusted slightly to optimize the match with observed olivine phenocryst compositions. Additionally, whole rock NiO contents often provide unreliable primary magma NiO contents due to olivine sorting; for primary magmas of peridotite-sources, we use Ni (ppm) = $21.6MgO - 0.32MgO^2 + 0.051MgO^3$ (Herzberg, 2011).

From these identified primary magmas, both olivine and clinopyroxene were permitted to crystallize along a liquid line of descent. The Ol:Cpx proportions have been varied arbitrarily because the exact T-P paths at which melts interact with wall rocks are not known. We assume perfect fractional crystallization, and the extraction of olivine and clinopyroxene was accomplished computationally by removing them incrementally by 0.1%. Of course, the compositions of olivine and clinopyroxene need to be computed at each step in order to

compare with observed phenocryst compositions. This is accomplished with partition coefficients as discussed now.

The method for computing the compositions of Ni, Ca, Mn, and Fe in olivine in equilibrium with both the primary magmas and their derivative liquids was reported in Herzberg (2011), and is repeated here because it is an appropriate introduction to the calculation of clinopyroxene composition. As discussed above, we make use of the partition coefficient:

$$D_i^{Ol/L} = X_i^{Ol} / X_i^{L} \quad (9)$$

where X_i refers to the mole fraction of oxide component i in the phases liquid (L), olivine (Ol), based on one metal cation per oxide (i.e., SiO_2, MgO, $AlO_{1.5}$, $NaO_{0.5}$ etc.). We used the temperature-independent Beattie-Jones parameterization model (Jones, 1984; Beattie et al., 1991):

$$D_i^{Ol/L} = A_i^{Ol/L} D_{MgO}^{Ol/L} + B_i^{Ol/L} \quad (10)$$

where $D_{MgO}^{OL} = MgO^{Ol}/MgO^{L}$ and the A and B constants have been parameterized from experimental data. Parameterized results for Ni reported by Beattie *et al*. (1991) were discussed above (equation 3). Results for Mn and Ca are from Herzberg and O'Hara (2002), and we use a 1 atmosphere Fe/Mg exchange coefficient from Toplis (2005).

The method for calculating Cpx fractionation is similar to that for Ol addition/subtraction calculations (Herzberg and Asimow, 2008; Herzberg, 2011) except that the partition coefficients are different. We have parameterized high quality high pressure experimental data for Cpx/L from the following sources: Walter (1998), Longhi (2002), Pertermann and Hirschmann (2003), Keshav et al. (2004), Gerbode and Dasgupta (2010) and Le Roux et al. (2011). For Fe and Mn, we follow the Jones-Beattie method of parameterizing partition coefficients as discussed above for olivine:

$$D_{FeO}^{Cpx/L} = 0.215\, D_{MgO}^{Cpx/L} + 0.181 \quad (R = 0.98) \quad (11)$$

$$D_{MnO}^{Cpx/L} = 0.284\, D_{MgO}^{Cpx/L} + 0.294 \quad (R = 0.91) \quad (12)$$

and

$$D_{CaO}^{Cpx/L} = 0.395\, D_{MgO}^{Cpx/L} + 0.503 \quad (R = 0.85) \quad (13)$$

where R refers to the correlation coefficient. Results show that D for FeO and MnO are well-correlated with D for MgO (Fig. S5), as indicated also by the high correlation coefficients. Equations (11) and (12) describe equally well the partitioning of Fe and Mn in melting experiments for which 3-4% H_2O was reported in the liquid (Balta et al., 2011). However, as discussed by Balta et al. (2011), clinopyroxene in these wet experiments contain unusually high CaO compared with anhydrous experiments; as it is not likely that intraplate magmas are this wet (Herzberg and Asimow, 2008), the Balta results for CaO were not included in the parameterization. For all other experiments, the lower correlation coefficients for CaO may result in part from vacant sites (Hirschmann and Petermann, 2003). But there are also less satisfactory correlations of $D_{MgO}^{Cpx/L}$ with Ds for TiO_2, $AlO_{1.5}$, and $NaO_{0.5}$, indicating limitations

in application of the Jones-Beattie method to coupled ionic substitutions. Improved correlations were obtained empirically with the following equations:

$$D_{TiO2}^{Cpx/L} = 0.215\ D_{CaO}^{Cpx/L} - 0.047 \qquad (R = 0.87) \qquad (14)$$

$$D_{AlO1.5}^{Cpx/L} = -1.114\ D_{SiO2}^{Cpx/L} + 1.859 \qquad (R = 0.77) \qquad (15)$$

and

$$D_{NaO0.5} = 1.304\ D_{AlO1.5}^{Cpx/L} - 0.412 \qquad (R = 0.93) \qquad (16)$$

D values for CaO, SiO_2 $AlO_{1.5}$, and $NaO_{0.5}$ are computed from mole fractions of these components in Cpx and Liquid in the usual manner; however, sodium partitioning depends on aluminum partitioning and equation (15) must be solved before equation (16).

Clinopyroxene compositions that were computed with the above partition coefficients were assumed to be stoichiometric, with no site vacancies, and all plot exactly within the pyroxene-garnet plane.

It is useful to compare the partitioning behavior of garnet and clinopyroxene, and results are shown in Fig. S5 and listed below.

	$A^{Gt/L}$	$B^{Gt/L}$	R (correlation coefficient)
FeO	0.589	-0.135	0.99
MnO	1.169	-0.375	0.98
CaO	0.20	0.31	0.96
NiO (see below)			

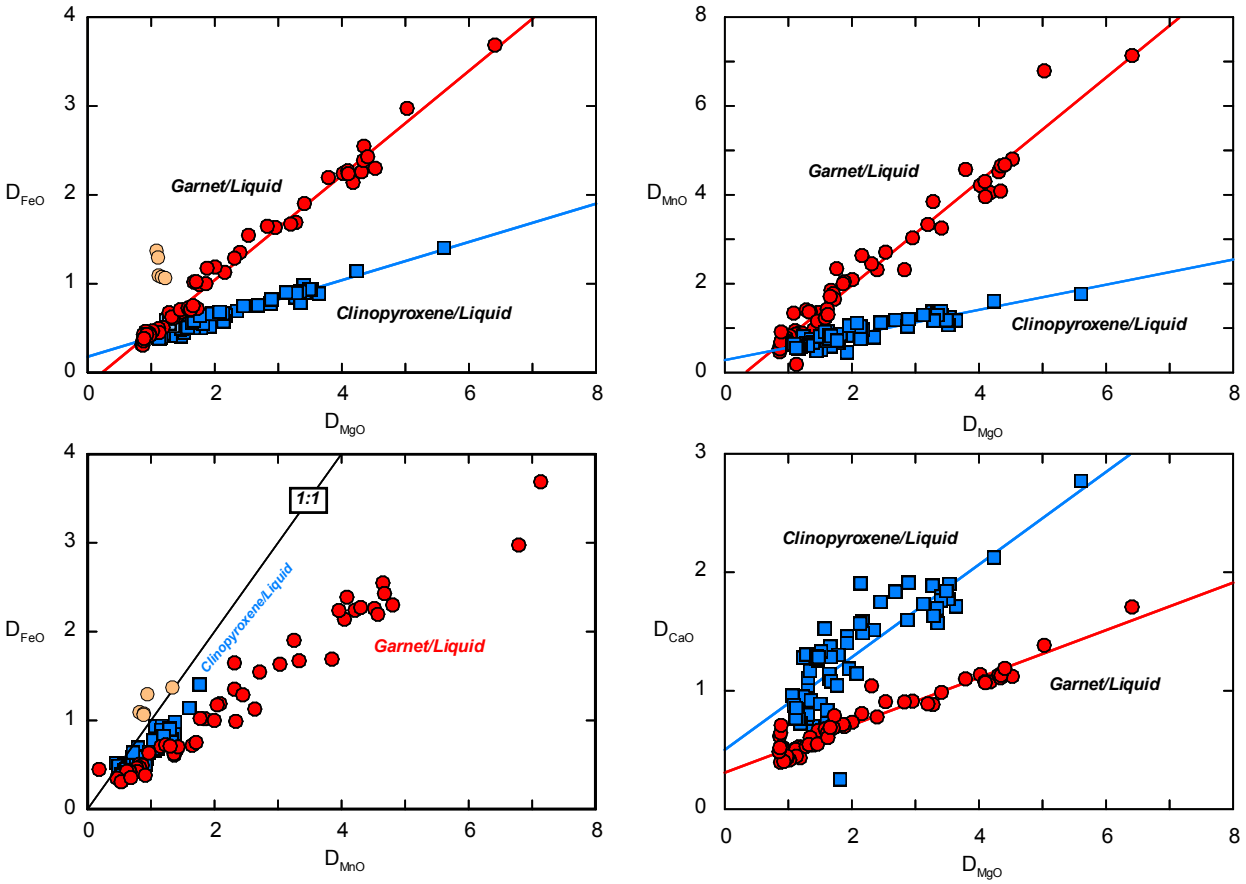

Figure S5. Partition coefficients determined for clinopyroxene/liquid (blue squares) and garnet/liquid (red circles) from experimental data listed in the text. Note that FeO contents of garnets in experimental data from Keshav et al.(2004; orange circles) are highly discrepant, unlike MnO, and were not included in the regression.

Included in Fig. S5 are data for majorite garnet/liquid from experiments in the range 15.5-22.5 GPa and 2135-2375°C (Herzberg and Zhang, 1996). These extreme T-P data are fully consistent with others in the 2.5 to 7.0 GPa range, demonstrating the success of the Jones-Beattie model in capturing the partitioning of Fe, Mn, Mg, and Ca between garnet and liquid over all conditions of magma genesis.

Manganese is strongly partitioned into garnet, whereas it displays both compatible and incompatible behavior in clinopyroxene. Furthermore, MnO is more compatible in Cpx and Gt than is FeO (Fig. S5). The ability of garnet and clinopyroxene to preferentially accept Mn over Fe during melting and crystallization will yield liquids with elevated Fe/Mn. Olivines that crystallize from such liquids will also be elevated in Fe/Mn and can indicate a garnet pyroxenite source during partial melting (Sobolev et al., 2007; Herzberg, 2011). Alternatively, olivines with elevated Fe/Mn can indicate garnet pyroxenite crystallization from melts of a peridotite source.

There are very few experiments that constrain the partitioning of Ni for Cpx/L and Gt/L. However, Canil (1999) reported variable $D_{NiO}^{Gt/Ol}$ in subsolidus experiments, reaching a

maximum of 0.11 at 1500°C and 5 GPa. Using Canil's data, Sobolev et al. (2005) estimated $D_{NiO}^{Gt/Ol}$ in the 0.10-0.14 range appropriate to Walter's (1998) experiments for which no NiO data were reported; similarly, they estimated $D_{NiO}^{Gt/Cpx}$ of about 0.5. For the case of L + Ol + Cpx ± Gt, we can estimate $D_{NiO}^{Cpx/L}$ and $D_{NiO}^{Gt/L}$ from $D_{NiO}^{Gt/Ol}$ and $D_{NiO}^{Cpx/Ol}$ and $D_{NiO}^{Ol/L}$ (Beattie et al., 1991; equation 1). Results are:

$$D_{NiO}^{Cpx/Ol} = 0.250\ D_{NiO}^{Ol/L} \quad (17)$$

and

$$D_{NiO}^{Gt/L} = 0.125\ D_{NiO}^{Ol/L} \quad (18)$$

There is only one experiment for which high quality Ni data are reported for all phases for L + Ol + Cpx, that being G107 of Le Roux et al. (2011). Results show $D_{NiO}^{Cpx/Ol} = 0.28\ D_{NiO}^{Ol/L}$ using Ni in olivine and liquid in experiment G107. The distribution of Ni between Ol and L in this experiment (8.32) is in good but not perfect agreement with the parameterization of Beattie et al. (1991; 9.32) at the $D_{MgO}^{Ol/L}$ in G107 (3.88). Using Beattie's parameterized $D_{NiO}^{Ol/L}$, we obtain for experiment G107 $D_{NiO}^{Cpx/Ol} = 0.250\ D_{NiO}^{Ol/L}$, in excellent agreement with equation (17).

5. Olivine Phenocrysts from Isla Gorgona, Ontong Java Plateau and Fernandina

Olivine phenocryst compositions from Isla Gorgona komatiites were provided by Sobolev et al. (2007) and are shown in Fig. S6. These have very high *Mg*-numbers, similar to those expected for early crystals from the primary magmas, and peridotite source provenance is indicated by Ca, Mn, and Fe/Mn (Herzberg, 2011; Sobolev et al., 2007). However, they distinctly enriched in Ni, and require crystallization of magmas of a Ni-rich peridotite source.

Olivine phenocryst compositions from the Ontong Java Plateau were also provided by Sobolev et al. (2007) and are also shown in Fig. S6. They have lower *Mg*-numbers than olivines from Gorgona, and there is some indication that both olivine and clinopyroxene fractionation has affected their compositions. Relative to olivine-only fractionation, the effects of variable clinopyroxene fractionation is to lower Ca and Mn, and raise both Ni and Fe/Mn.

Olivine phenocryst compositions for Fernandina are new and reported in Table S2 and shown in Fig. S7. These were obtained from a submarine sample D38A from Fernandina in the Galapagos Islands (Geist et al., 2006). Major and trace element data were obtained using the method of Sobolev 2007 on Rutgers University's Joel JXA-8600 electron microprobe. Detection limits were obtained from the Probe for Windows for all elements. Average detection limits for Si, Mg and Fe are 53, 36 and 40 ppm respectively. Average detection limits for trace elements Ni, Mn and Ca are 26, 28 and 16 ppm respectively. 2σ error for all elements was calculated from repeated analyses of the San Carlos olivine standard. Analyses of Si, Mg and Fe have a relative 2σ error of ~1.75%, ~0.51% and ~0.57% respectively. Analyses of trace elements Ni, Mn and Ca have a relative 2σ error of 2.02%, 2.68% and 3.06% respectively. The relative 2σ error for the Fo# is ~0.12%. Analyses with oxide totals > ± 2% deviation from 100% were excluded. Chemical formulas were calculated for all analyses. Analyses with deviations in stoichiometry > ± 1% were excluded. Relative to olivine-only fractionation, the effects of variable clinopyroxene fractionation (Geist et al., 1998) is to lower Ca and Mn, and raise both Ni and Fe/Mn.

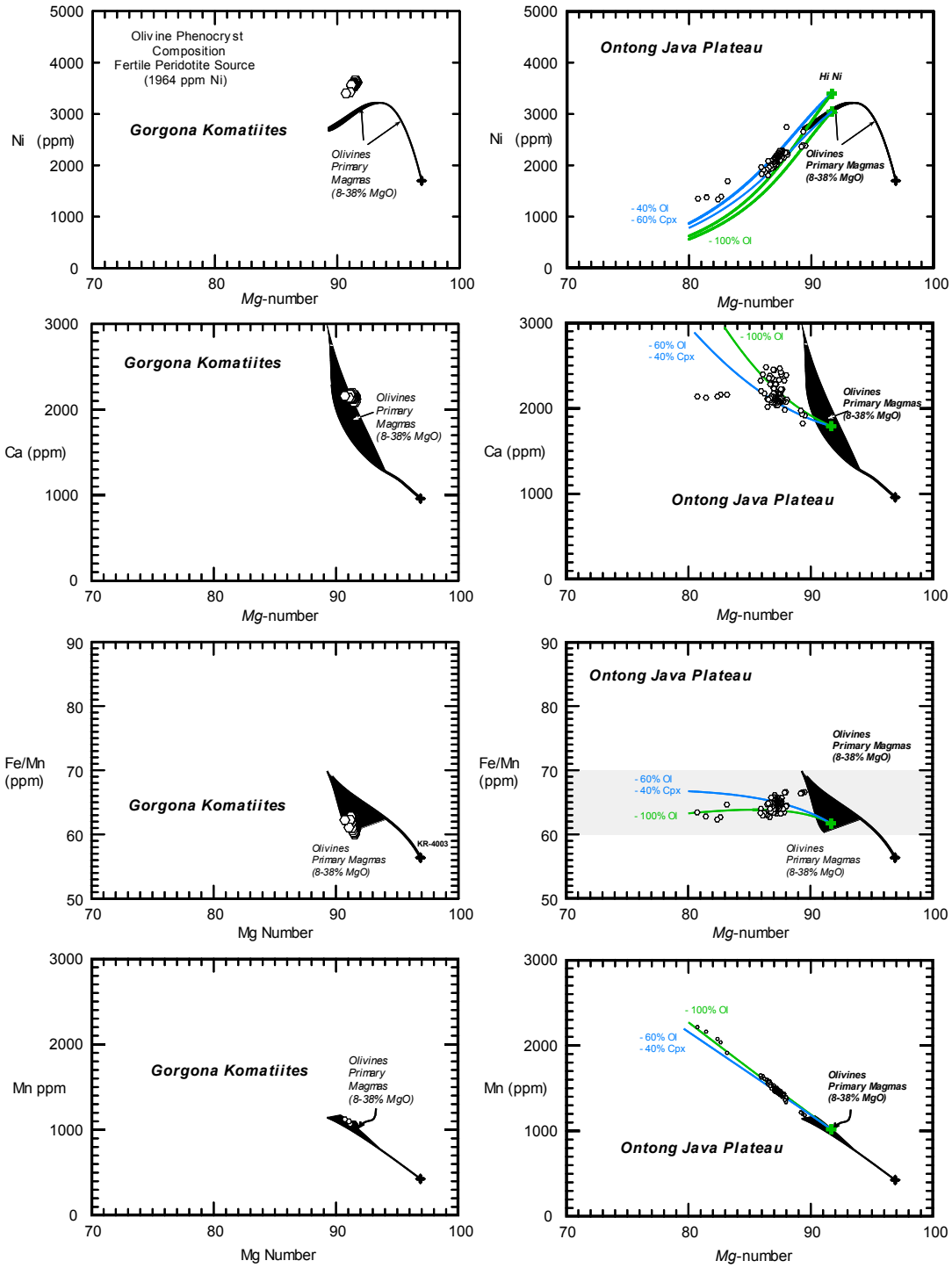

Figure S6. Mg-numbers and Ni, Ca, Mn, and Fe/Mn for calculated olivine (Herzberg, 2011) and observed olivine phenocrysts from Gorgona komatiites and basalts from the Ontong Java Plateau (Sobolev et al., 2007). Black regions are calculated olivines from primary magmas of peridotite (Herzberg, 2011). Green and blue lines are olivine compositions that crystallize from primary magmas that fractionated olivine and clinopyroxene in the weight proportions indicated. Hi Ni refers to olivine crystallization from a primary melt of a high Ni mantle peridotite.

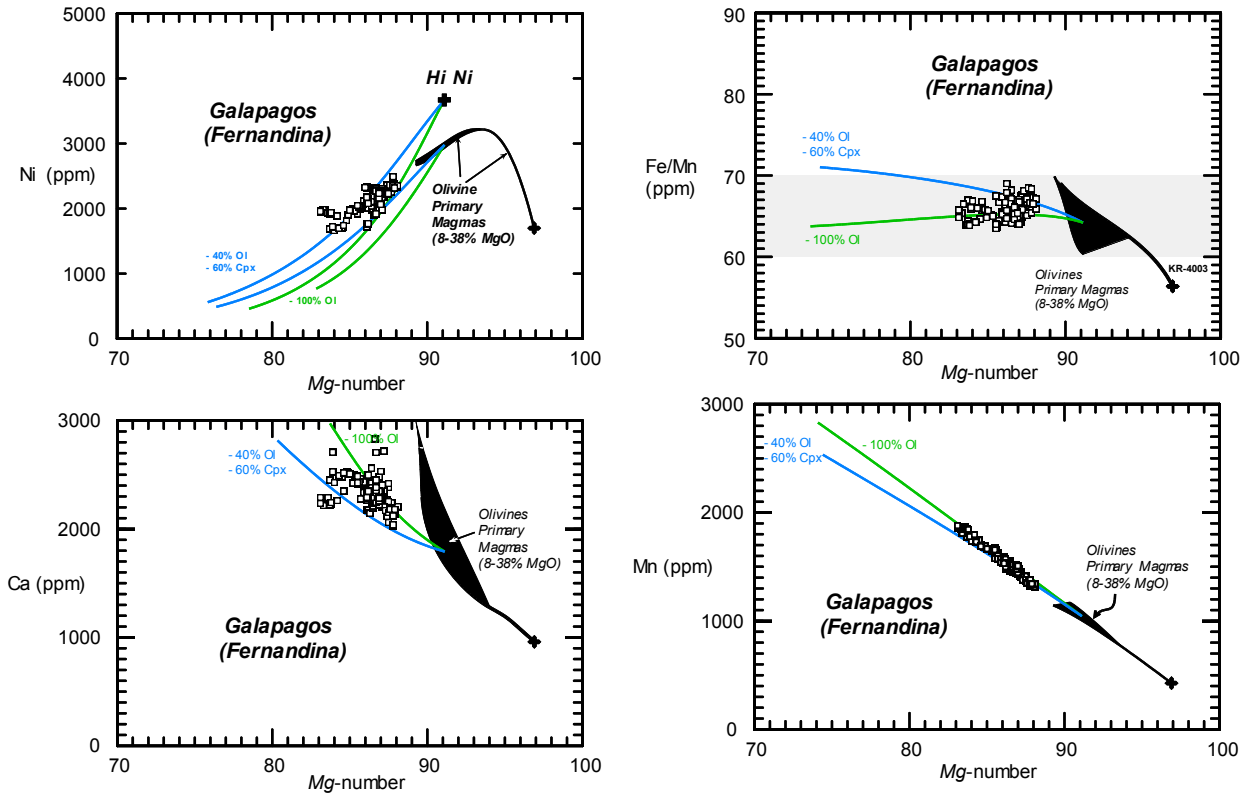

Figure S7. Mg-numbers and Ni, Ca, Mn, and Fe/Mn for calculated olivine (Herzberg, 2011) and observed olivine phenocrysts from a submarine sample D38A from Fernandina in the Galapagos Islands (Table S1). Black regions are calculated olivines from primary magmas of peridotite (Herzberg, 2011). Green and blue lines are olivine compositions that crystallize from primary magmas that fractionated olivine and clinopyroxene in the weight proportions indicated. Hi Ni refers to olivine crystallization from a primary melt of a high Ni mantle peridotite.

6. Examples of Peridotite and Pyroxenite Source Lithologies Inferred from Olivine Phenocryst Composition

Comparably high mantle potential temperatures have been inferred for both Hawaii and West Greenland occurrences (T_P = 1500-1600°C; Herzberg and Asimow, 2008; Herzberg and Gazel, 2009), and both erupted over thick lithosphere (Larsen and Pedersen, 2000; Li et al., 2000; 2004). If elevated temperature and pressure is the main mechanism for producing olivine phenocyrsts with high Ni contents, then it is to be expected olivine phenocryst compositions from Hawaii and West Greenland occurrences will have similar Ni, Mn, Fe/Mn, and Ca. This is not observed (Fig. S8). Hawaiian olivines are higher in Ni by ~ 1000 ppm, they are substantially lower Ca and Mn and higher Fe/Mn compared with those from West Greenland, Baffin Island and Disko Island.

Olivine phenocrysts from Alexo komatiites of Archean age have Ni contents that are somewhat higher than those of expected from olivines of primary peridotite-source magmas with 26-30% MgO (Fig. S9). However, the effect of minor olivine fractionation is to initially raise Ni then lower it, producing an array that is concaved toward the Mg-number axis (Herzberg, 2011). This sense of curvature computed from the Beattie-Jones Ni partitioning model is captured in olivines from Alexo (Fig. S9), a remarkable level of agreement. It is also clear from Fig. S9 that olivine phenocrysts from Hawaii and Alexo komatities have very different Ca, Mn, and Fe/Mn. For Alexo, a peridotite source provenance is clearly indicated (Fig. S9). In contrast, low Ca and Mn and high Fe/Mn for Hawaiian olivines are not consistent with peridotite-source melting.

Olivine phenocrysts in subduction zone andesites from the Mexican Volcanic Belt have the highest Ni contents ever reported (Straub et al., 2008), and greatly exceed the Ni contents of normal mantle peridotite (Fig. S10). Straub et al. (2008) interpreted these high Ni contents with a pyroxenite source lithology that formed by reaction of SiO_2-rich slab fluids with peridotite in the mantle wedge. Ni maxima are observed for 4 sub parallel arrays, and those with the lowest Mg-numbers exclude the possibility of formation from a peridotite source lithology. Most relevant to the present discussion is that it is not probable that these olivine Ni contents can be interpreted by any temperature- and pressure-melting and crystallization process that operated on a normal Ni peridotite source.

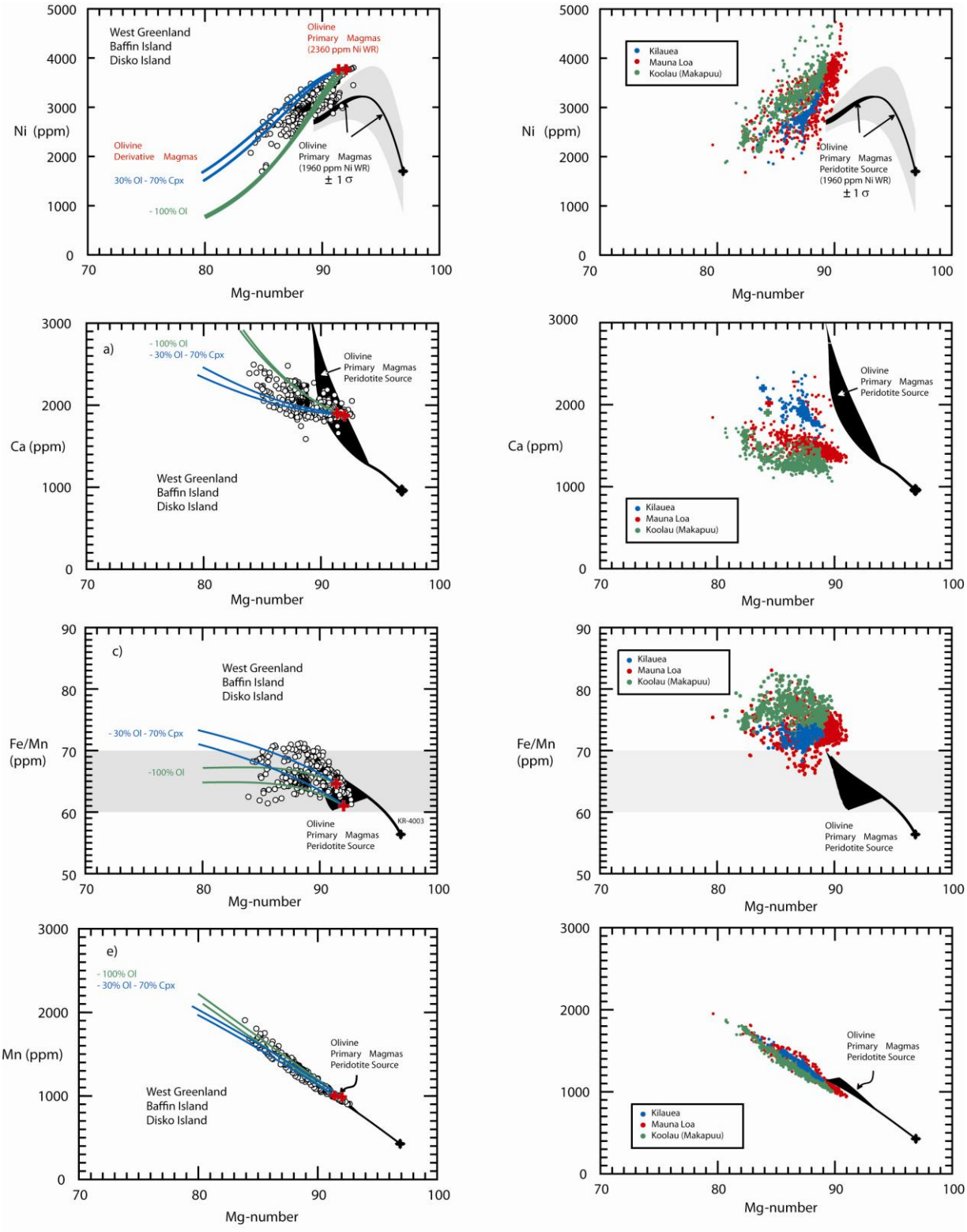

Figure S8. A comparison of olivine phenocryst compositions for Hawaii, West Greenland, Baffin Island and Disko Island. All data are from Sobolev et al. (2007).

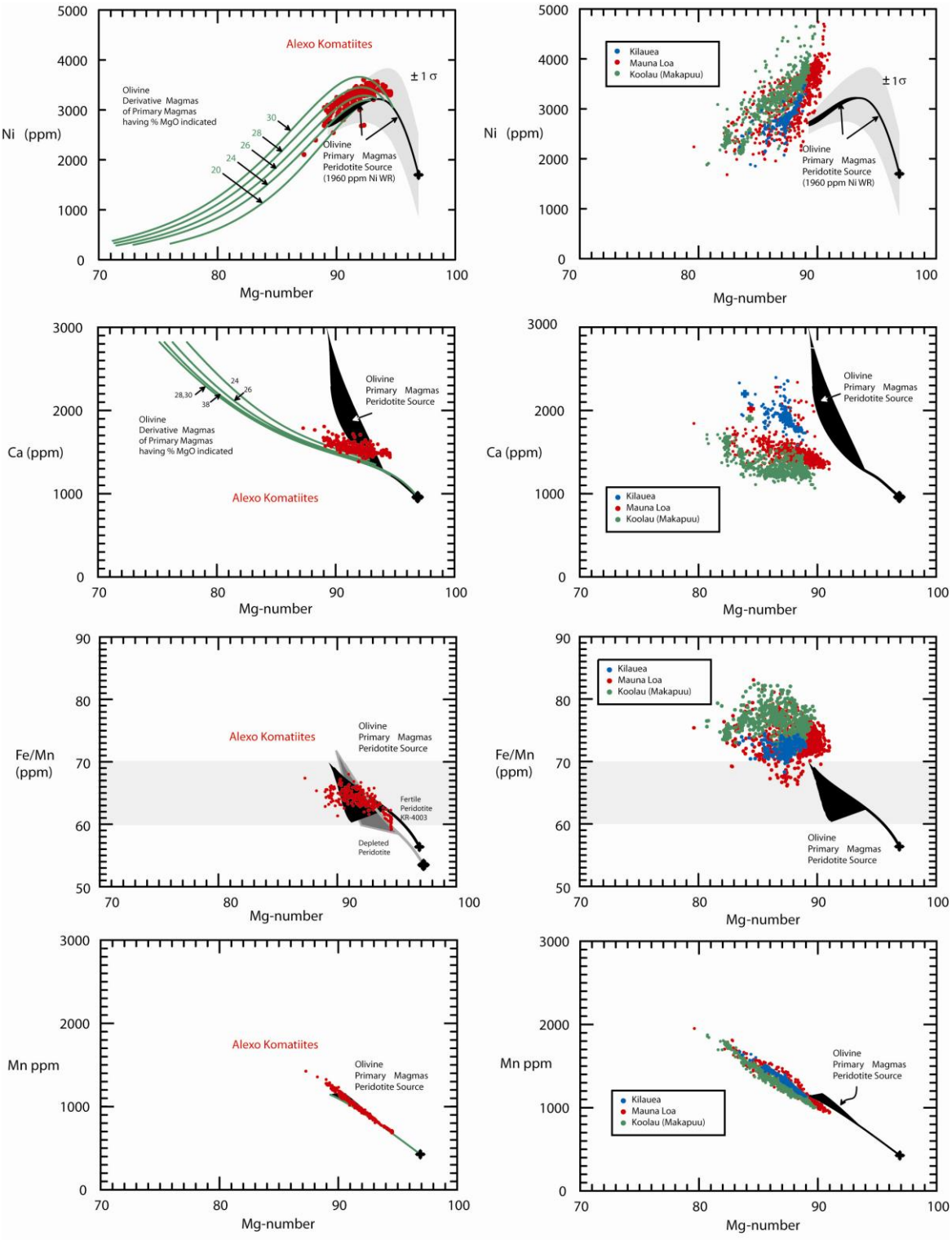

Figure S9. A comparison of olivine phenocryst compositions for Hawaii and Alexo komatiites of Archean age. All data are from Sobolev et al. (2007).

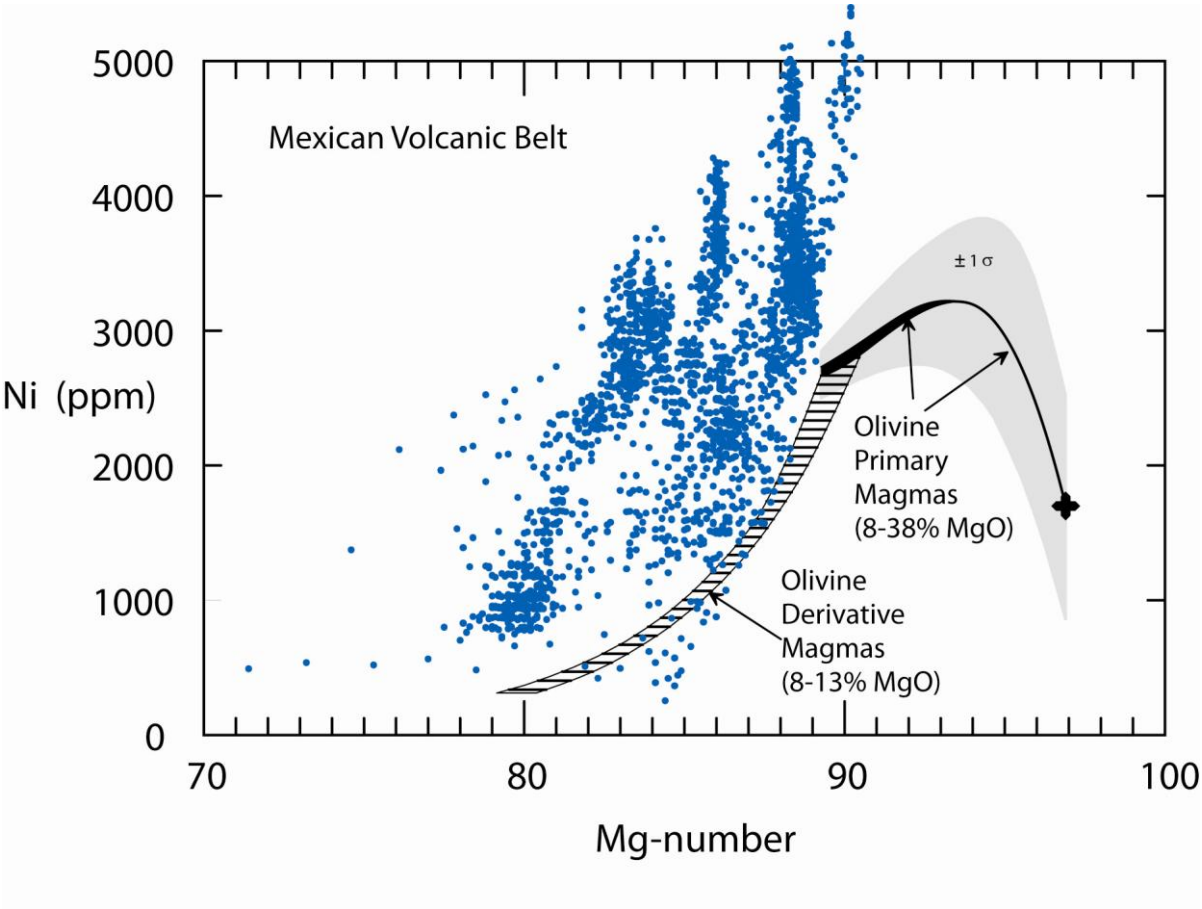

Figure S10. Olivine phenocryst compositions from the Mexican Volcanic Belt (Straub et al., 2008).

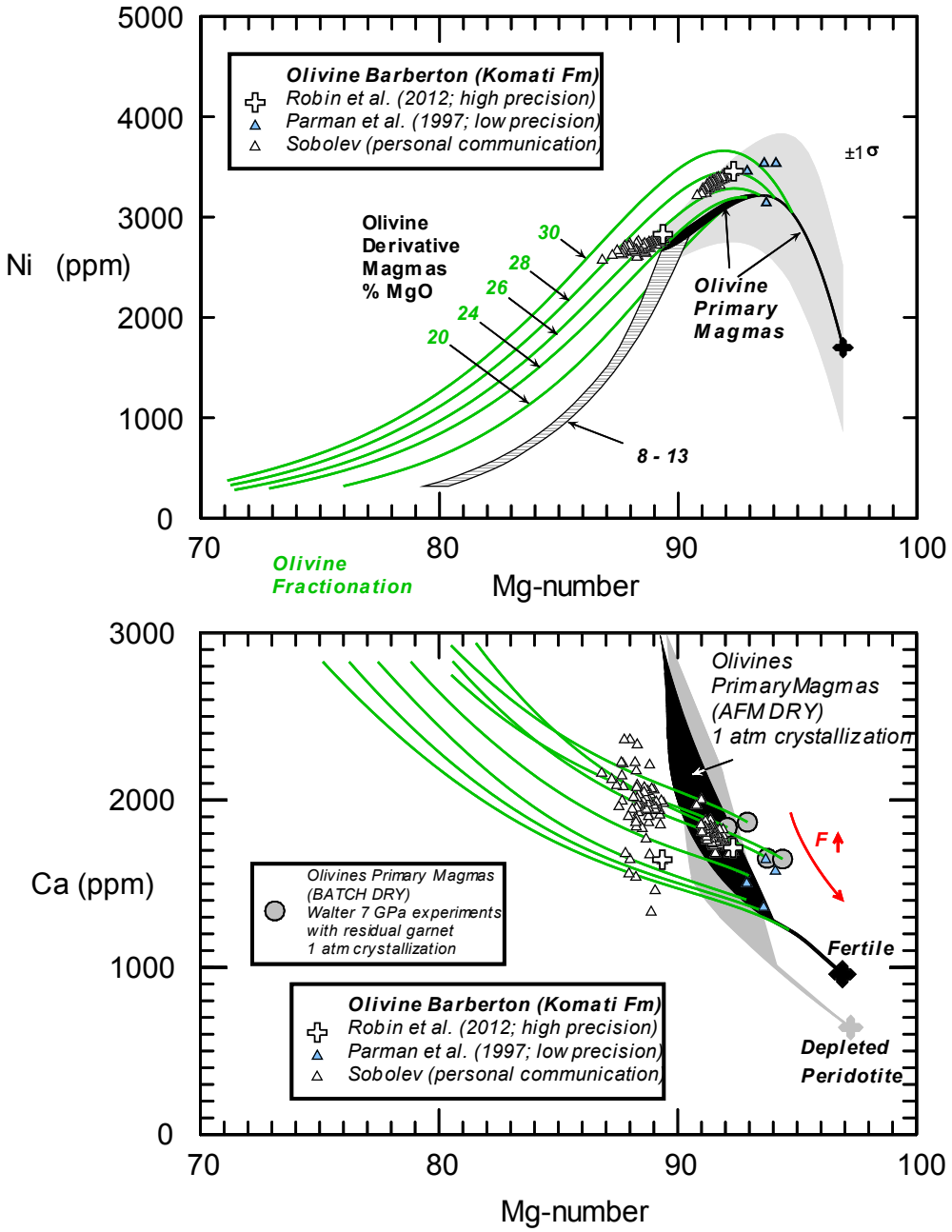

Figure S11. Olivine phenocryst compositions from the Komati Formation of the Barberton greenstone belt compared with olivines expected to crystallize from primary magmas of dry fertile peridotite (black form; 3.45% CaO). Red arrow labeled F reflects lower Ca content of olivine with increasing melt fraction F. Low Ca olivine outliers may have grown in heterogeneous melts formed at high melt fractions or from melts of more depleted peridotite (grey form; 2.14% CaO; melt solutions in Herzberg (2004b) except calculated for accumulated fractional melting). It is notable that depleted isotopic compositions do not correlate with depleted major element compositions of peridotite sources (e.g., Salters and Stacke, 2004), and the olivine Ca contents should cover the full range of possibilities. Model depleted and fertile peridotite compositions have ~ 8% FeO (Herzberg and O'Hara, 2002). An ancient FeO-depleted source is expected to yield olivines with similar CaO but higher Mg-numbers.

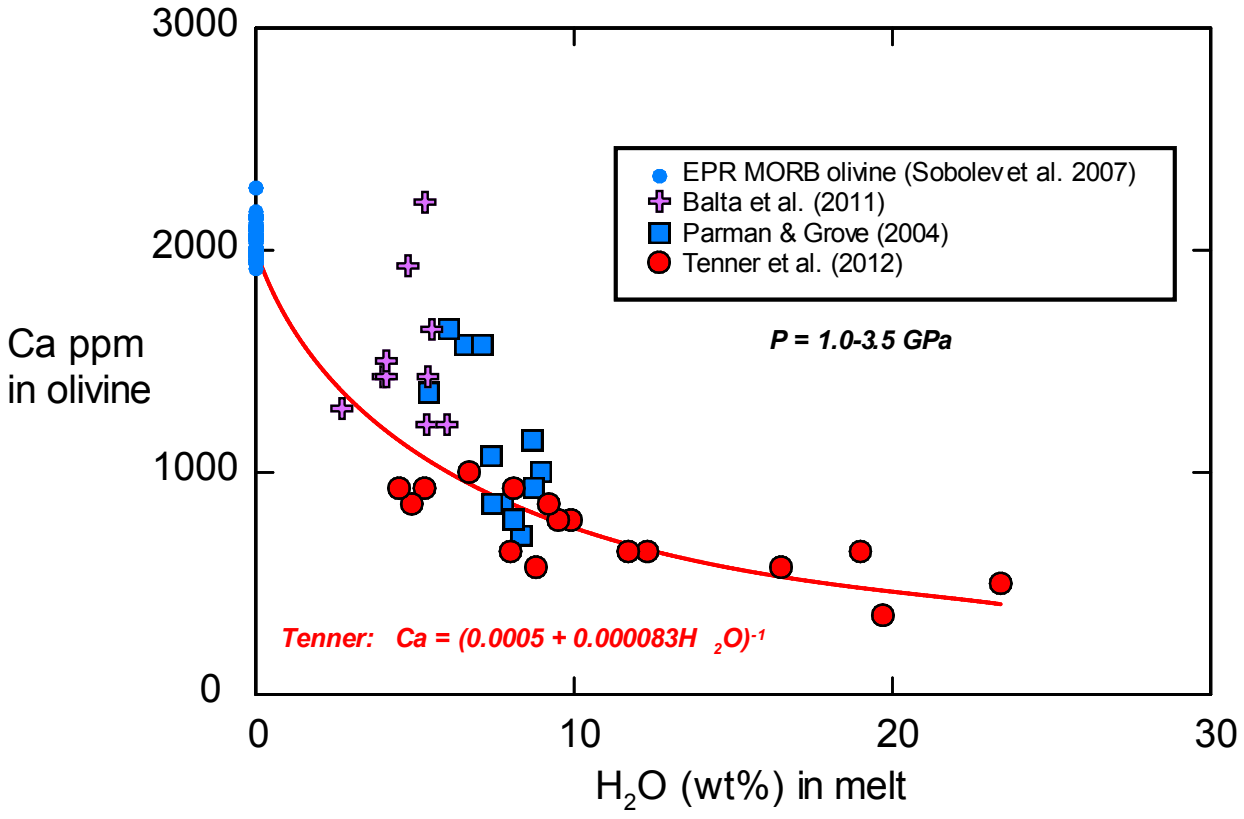

Figure S12. Ca contents of olivine in experimental melts with various H_2O contents.

References

Albarède, F., B. Luais, G. Fitton, M. Semet, E. Kaminski, B.G.J. Upton, P. Bachèlery, and Cheminée, J.-L. (1997). The geochemical regimes of Piton de la Fournaise volcano (Réunion) during the last 530000 years. *Journal of Petrology* ***38***, 171-201.

Balta, J.B., Asimow, P.D. and Mosenfelder, J.L. (2011). Hydrous, low-carbon melting of garnet peridotite. *Journal of Petrology* **52**, 2079-2105.

Beattie, P., Ford, C. and Russell, D. (1991). Partition coefficients for olivine-melt and orthopyroxene-melt systems. *Contributions to Mineralogy and Petrology* **109**, 212-224.

Canil, D. (1996). The Ni-in-garnet geothermometer: calibration at natural abundances. *Contributions to Mineralogy and Petrology* **136**, 240-246.

Filiberto, J., Jackson, C., Le, L. and Treiman, A.H. (2009). Partitioning of Ni between olivine and an iron-rich basalt: experiments, partition models, and planetary implications. American Mineralogist 94, 256-261.

Geist, D., Naumann, T. and Larson, P. (1998). Evolution of Galapagos magmas: mantle and crustal fractionation without assimilation. *Journal of Petrology* **39**, 953-971.

Geist, D., Fornari, D.J., Kurz, M.D., Harpp, K.S., Soule, S.A., Perfit, M.R. and Koleszar, A.M. (2006). Submarine Fernandina: Magmatism at the leading edge of the Galápagos hot spot. *Geochemistry Geophysics Geosystems* **7**, Q12007, doi:10.1029/2006GC001290.

Gerbode, C. and Dasgupta, R. (2010). Carbonate-fluxed melting of MORB-like pyroxenite at 2.9 GPa and genesis of HIMU ocean island basalts. *Journal of Petrology* **51**, 2067-2088.

Hart, S.R. and Davis, K.E. (1978). Nickel partitioning between olivine and silicate melt. *Earth and Planetary Science Letters* **40**, 203-219.

Herzberg, C.T. (1993) Lithosphere peridotites of the Kaapvaal craton. *Earth and Planetary Sciences Letters* **120**, 13-29.

Herzberg, C. (1999). Phase equilibrium constraints on the formation of cratonic mantle. In: *Mantle Petrology: Field Observations and High Pressure Experimentation: A Tribute to Francis R. (Joe) Boyd.* The Geochemical Society, Special Publication 6, Fei, Y., Bertka, C.M., Mysen, B.O., eds, 241-257.

Herzberg, C. (2004a). Partial crystallization of mid-ocean ridge basalts in the crust and mantle. *Journal of Petrology* **45**, 2389-2405.

Herzberg, C. (2004b). Geodynamic information in peridotite petrology. *Journal of Petrology* **45**, 2507-2530.

Herzberg, C. (2011). Identification of Source Lithology in the Hawaiian and Canary Islands: Implications for Origins. *Journal of Petrology* **52**, 113-146.

Herzberg, C. and Zhang, J. (1996). Melting experiments on anhydrous peridotite KLB-1: Compositions of magmas in the upper mantle and transition zone. *Journal of Geophysical Research* **101**, 8271-8295.

Herzberg, C. and O'Hara, M.J. (2002). Plume-associated ultramafic magmas of phanerozoic age. *Journal of Petrology* **43**, 1857-1883.

Herzberg, C. and Asimow, P.D. (2008). Petrology of some oceanic island basalts: PRIMELT2.XLS software for primary magma calculation. *Geochemistry Geophysics Geosystems* **8**, Q09001, doi:10.1029/2008GC002057.

Ionov, D.A. (2007). Compositional variations and heterogeneity in fertile lithospheric mantle: peridotite xenoliths in basalts from Tariat, Mongolia. *Contributions to Mineralogy and Petrology* **154**, 455–477.

Ionov, D.A. (2010) Petrology of mantle wedge lithosphere: New data on supra-subduction zone peridotite xenoliths from the andesitic Avacha volcano, Kamchatka. *Journal of Petrology* **51,** 327-361.

Ionov, D.A., Ashchepkov, I. and Jagoutz, E. (2005). The provenance of fertile off-craton lithospheric mantle: Sr-Nd isotope and chemical composition of garnet and spinel peridotite xenoliths from Vitim, Siberia. *Chemical Geology* **217**, 41-74.

Ionov, D.A., Prikhodko, V., Bodinier, J.-L., Sobolev, A.V. and Weis, D. (2005). Lithospheric mantle beneath the south-eastern Siberian craton: petrology of peridotite xenoliths in basalts from the Tokinsky Stanovik. *Contributions to Mineralogy and Petrology* **149**, 647-665.

Ionov, D.A. and Hofmann, A.W. (2007). Depth of formation of subcontinental off-craton peridotites. *Earth and Planetary Science Letters* **261**, 620-634.

Jones, J.H. (1984). Temperature and pressure- independent correlations of olivine-liquid partition coefficients and their application to trace element partitioning. *Contributions to Mineralogy and Petrology* **88**, 126-132.

Keshav, S., Gudfinnsson, G.H., Sen, G. and Fei, Y.-W. (2004). High-pressure melting experiments on garnet clinopyroxenite and the alkalic to tholeiitic transition in ocean-island basalts. *Earth and Planetary Science Letters* **223**, 365-379.

Larsen, L.M. and Pedersen, A.K. (2000). Processes in high-Mg, high-T magmas: evidence Fro m olivine, chromite and glass in Palaeogene picrites from West Greenland. *Journal of Petrology* **41**, 1071-1098.

Le Roux, V., Dasgupta, R. and Lee, C.-T.A. (2011). Mineralogical heterogeneities in the Earth's mantle: Constraints from Mn, Co, Ni and Zn partitioning during partial melting. *Earth and Planetary Science Letters* **307**, 395-408.

Li, X., Kind, R., Priestley, K., Sobolev, S.V., Tilmann, F., Yuan, X. and Weber, M. (2000). Mapping the Hawaiian plume conduit with converted seismic waves. *Nature* **405**, 938-941.

Li, X. Kind, R. Yuan, X., Wölbern, I. and Hanka, W. (2004). Rejuvenation of the lithosphere by the Hawaiian plume. *Nature* **427**, 827-829.

Li, C. amd Ripley, E.M. (2010). The relative effects of composition and temperature on olivine-liquid Ni partitioning: Statistical deconvolution and implications for petrologic modeling. *Chemical Geology* **275**, 99-104.

Longhi, J. (2002), Some phase equilibrium systematics of lherzolite melting: I, *Geochemistry Geophysics Geosystems* **3**, 10.1029/2001GC000204.

Longhi, J., Durand, S.R. and Walker, D. (2010). The pattern of Ni and Co abundances in lunar olivines. *Geochimica et Cosmochimica Acta* **74**, 784-798.

Matzen, A.K., Baker, M.B., Beckett, J.R. and Stolper, E.M. (2011). Fe-Mg Partitioning between olivine and high-magnesian melts and the nature of Hawaiian parental liquids. *Journal of Petrology* **52**, 1243-1263.

Niu, Y., Wilson, M., Humphreys, E.R. and O'Hara, M.J. (2011). The origin of intra-plate ocean island basalts (OI B): the lid effect and its geodynamic implications. *Journal of Petrology* **52**, 1443-1468.

O'Hara, M.J. (1968). The bearing of phase equilibria studies in synthetic and natural systems on the origin of basic and ultrabasic rocks. *Earth Science Reviews* **4**, 69-133.

Pertermann, M. and Hirschmann, M.M. (2003). Anhydrous partial melting experiments on MORB-like eclogite: phase relations, phase compositions and mineral-melt partitioning of major elements at 2-3 GPa. *Journal of Petrology* **44**, 2173-2201.

Putirka, K.D., Ryerson, F.J., Perfit, M. and Ridley, W.I. (2011). Mineralogy and composition of oceanic mantle. *Journal of Petrology* **52**, 279-313.

Salters, V.J.M and Stracke, A. (2004). Composition of depleted mantle. *Geochemistry,Geophysics, Geosystems* **5**, Q05004, doi:10.1029/2003GC000597.

Sobolev, A.V., Hofmann, A.W., Sobolev, S.V. and Nikogosian I.K. (2005). An olivine-free mantle source of Hawaiian shield basalts. *Nature* **434**, 590-597.

Sobolev, A.V., Hofmann, A.W., Kuzmin, D.V., Yaxley, G.M., Arndt, N.T., Chung, S.-L., Danyushevsky, L.V., Elliott, T., Frey, F.A., Garcia, M.O., Gurenko, A.A., Kamenetsky, V.S., Kerr, A.C., Krivolutskaya, N.A., Matvienkov, V.V., Nikogosian, I.K., Rocholl, A., Sigurdsson, I.A., Sushchevskaya, N.M. and Teklay M. (2007). The amount of recycled crust in sources of mantle-derived melts. *Science* **316**, 412-417.

Straub, S.M., LaGatta, A.B., Pozzo, A.L.M.-D. and Langmuir, C.H. (2008). Evidence from high Ni olivines for a hybridized peridotite/pyroxenite source for orogenic andesites from the central Mexican Volcanic Belt. *Geochemistry Geophysics Geosystems* **9**, Q03007, doi: 10.1029GC001583.

Taura, H., Yurimoto, H., Kurita, K. and Sueno, S. (1998). Pressure dependence on partition coefficients for trace elements between olivine and coexisting melts. *Physics and Chemistry of Minerals* **25**, 469-484.

Toplis, M.J. (2005). The thermodynamics of iron and magnesium partitioning between olivine and liquid: criteria for assessing and predicting equilibrium in natural and experimental systems. *Contributions to Mineralogy and Petrology* **149**, 22-39.

Wang, Z. and Gaetani, G.A. (2008). Partitioning of Ni between olivine and siliceous eclogite partial melt: experimental constraints on the mantle source of Hawaiian basalts. *Contributions to Mineralogy and Petrology* **156**, 661-678.